Computers and Geotechnics **7** (1989) 289–318

FINITE ELEMENT ANALYSIS OF A CENTRIFUGE MODEL OF A RETAINING WALL EMBEDDED IN A HEAVILY OVERCONSOLIDATED CLAY

M. D. Bolton and A. M. Britto
University Engineering Department
Cambridge University, Trumpington Street
Cambridge, CB2 1PZ, England

W. Powrie
Queen Mary College, University of London,
Mile End Road, London E1 4NS, England

T. P. White
Main Roads Department, Highway Authority
Western Australia

ABSTRACT

The current study is aimed at the behaviour right upto collapse of a retaining wall embedded in overconsolidated clay. It is found that the excess pore pressures generated due to the excavation are fairly well simulated. The rupture lines on the passive side in the centrifuge model test were closely matched by two lines along which the stress state was reaching the critical state in the analysis. The displacements on the active side were not well matched especially the vertical settlements near to the wall. The bending moments were significantly overpredicted. The prop force due to excavation was also overpredicted. This is to be expected because the prop was modelled as rigid in the analysis.

INTRODUCTION

Finite element analyses using critical state models [1] to represent the behaviour of normally consolidated and lightly overconsolidated clays have been successful in a variety of circumstances [2-4]. The present study attempts to evaluate the shortcomings (if any) of critical state concepts in modelling clays which are heavily overconsolidated, with reference to the particular problem of embedded cantilever in situ retaining walls. It is rarely possible to take a full-scale construction to failure : in this paper, therefore, the results of the finite element analysis are compared with data from a centrifuge model test.

In situ retaining walls, which are installed in the ground prior to excavation, are used in the construction of motorways, basements and other deep excavations, and cut and cover tunnels. The effect of the new excavation on the surrounding ground and existing buildings is minimised by the use of in situ methods: this is often of critical importance in built-up areas and city centres. In the

Computers and Geotechnics 0266-352X/89/$03·50 © 1989 Elsevier Science Publishers Ltd, England. Printed in Great Britain

proposed rail link between London and the channel tunnel, for example, cut and cover techniques are to be used quite extensively.

CENTRIFUGE MODEL TEST : SAMPLE PREPARATION AND EXPERIMENTAL PROCEDURE

The clay used in the centrifuge model test was Speswhite Kaolin prepared from a slurry having a water content of 120%. The slurry was poured into a consolidation press and was gradually compressed one dimensionally to an effective vertical stress of 1250 kPa. The sample was unloaded in stages to a vertical effective stress of 80 kPa. This vertical stress was then released, and the clay was removed from the consolidation press and cut to receive the model retaining wall. The model wall was made of 3/8 inch (9.5 mm) thick Dural aluminium alloy, giving a bending stiffness (EI) at prototype scale of 10^7 kNm^2/metre. The excavation was also made at this stage, the clay removed being replaced by a rubber bag filled with zinc chloride solution mixed at the same density as the clay.

The model was then placed in the centrifuge strong box and instrumented. A set of markers was placed on the face of the sample in a regular grid before the perspex window was bolted into position. This enabled photographs to be taken at regular intervals during the centrifuge test, which were used to measure the displacements which occurred.

The sample was reconsolidated in the centrifuge at 125 g, equilibrium conditions being reached with the water table at ground level prior to the simulation of excavation in front of the wall. The vertical stress history after reconsolidation corresponds to the removal of about 150 m of overlying soil at prototype scale.

The provision of a valve operated waste pipe enabled the zinc chloride solution to be dumped from the rubber bag simulating the process of excavation in front of the wall. Just prior to dumping the zinc chloride, the water table on the side to be excavated was drawn down to formation level. The water table on the retained side was maintained at ground level. Drainage of water was allowed from the base of the excavation, but no water was available if suction develops along this face. The layer of porous plastic at the base of the model was supplied with water at hydrostatic pressure corresponding to the water table at the ground surface during reconsolidation phase only : after excavation, it acted as an internal drain or equipotential.

In test DWC11, the diaphragm wall supported a retained height of 10 m (80 mm model scale) with a depth of embedment of 5 m at prototype scale. The wall was propped at the level of the retained soil surface. Fig. 1 shows the layout of the centrifuge package. Further details of this test, and of a straightforward limit analysis of its ultimate failure, were reported in Bolton and Powrie [5].

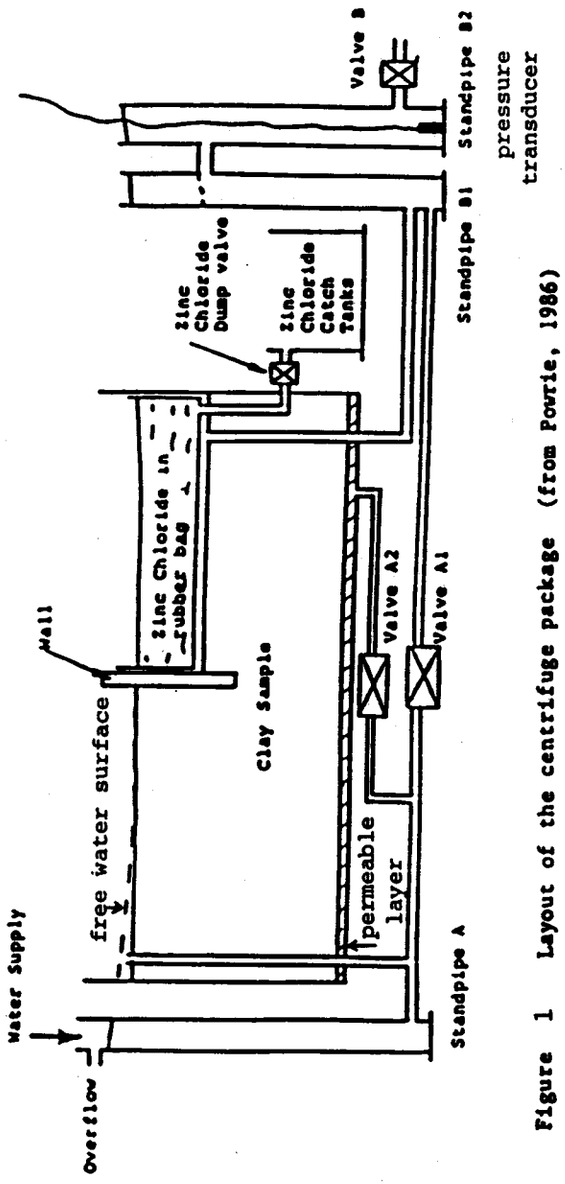

Figure 1 Layout of the centrifuge package (from Powrie, 1986)

ANALYSIS

Soil Model

Fig. 2 shows the Schofield soil model [6] which incorporates the Hvorslev surface on the dry side and Cam clay on the wet side. This model also includes a tension cut-off. It should be noted that the Hvorslev surface and the tension cut-off are treated as alternate yield surfaces on the dry side of critical states. In real soil when a stress path reaches the Hvorslev surface the soil ruptures in thin layers. However in the finite element formulation of the soil model, the surface is treated as a yield surface where plastic yielding takes place. This implementation on the dry side is used in preference to the Cam-clay and modified Cam clay because of the overestimation of the elastic response of these models on the dry side. For comparison the modified Cam-clay model is also shown in the above figure. The yield surfaces shown pass through a common stress point which corresponds to one dimensional consolidation. The Schofield soil model requires two more parameters than the Cam clay model. The slope of the Hvorslev surface in q-p' space along a constant volume line, H, is calculated from ϕ_H in a Mohr-Coulomb representation according to the equation :

$$\sin(\phi_H) = \frac{3H}{(6 + H)}$$

The slope of the tension cut-off line in q - p' space, S, was taken as 3 in the current analysis. A value of 2 would have been more appropriate because of the plane strain nature of the problem to be analysed. This is unlikely to have influenced the results.

M	= 0.9
λ	= 0.25 [7]
κ	= 0.05 [7]
Γ	= 3.48 [8]
ν'	= 0.33 [9]
k_v	= 0.66×10^{-9} m/s [10]
k_h	= 1.8×10^{-9} m/s [10]
H	= 0.59 (H = 0.76, $\phi_H = 19.8^0$ for triaxial extension)
γ	= 17.34 kN/m^3
γ_w	= 9.81 kN/m^3

TABLE 1 - Soil Parameters used in the Analysis

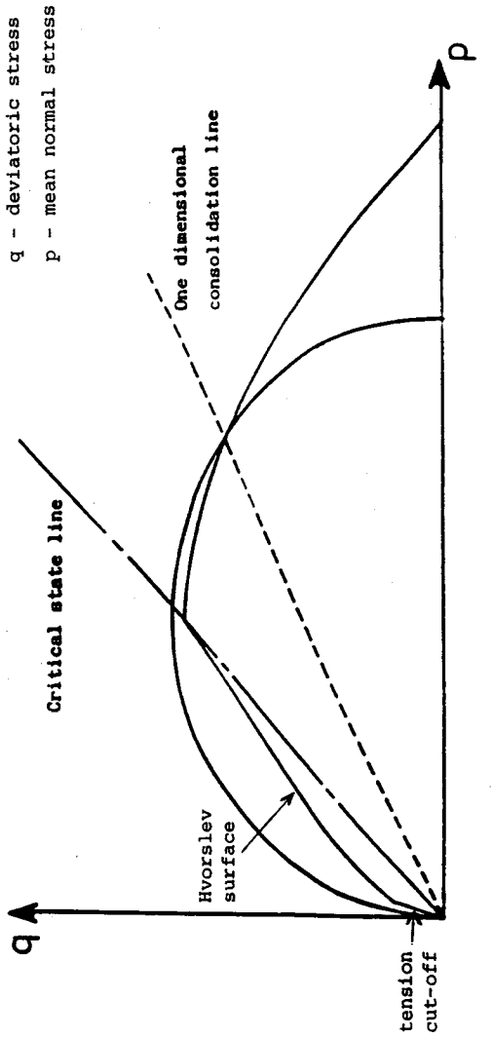

Figure 2 Matching the Modified Cam-clay and Schofield yield surfaces on the one dimensional consolidation line

Material Properties

The soil properties used in the analysis are detailed in Table 1. It was decided to allow the shear modulus to vary with the mean normal effective stress by using a constant value of Poisson's ratio ν'. The value of 0.33 is from Nadarajah's [9] data for spestone kaolin rather than the speswhite kaolin used in the current investigation but it has generally been found that the properties of the two types of kaolin are similar [11].

A series of triaxial tests on samples of speswhite kaolin cored from a large block which had been prepared in a manner similar to the centrifuge model gave a value for the Critical State friction parameter M of 0.84 [12]. This corresponds to a critical state angle of shearing in triaxial compression of about 22^{o}, which may be compared with a Hvorslev angle of shearing of about 20^{o} estimated by Stewart [13] on the basis of a series of strain-controlled drained triaxial swelling tests. This corresponds to an H value of 0.76. Fig. 3 shows the intersection of different yield surfaces on the π plane. Because of the plane strain nature of the problem, it was decided to adopt a critical state circle which touches the Mohr-Coulomb surface corresponding to the plane failure conditions. Accordingly M and H were reduced to 0.65 and 0.59 respectively. The diaphragm wall was modelled as linear elastic, with E' = $7x10^{7}$ kN/m^{2}, ν' = 0.33, and unit weight of 26.7 kN/m^{3}.

Finite Element Mesh

The finite element mesh used in the analysis [14] is shown in Fig. 4. 6 noded triangles were used to model the soil and 8 noded Quadrilaterals to model the diaphragm wall. A seven point integration rule was used for the triangle and a full 3 x 3 integration scheme was used for the quadrilaterals.

Slip elements of 0.1 mm thickness were used between the retaining wall and the soil to model the interface conditions which may permit relative slip. It also permits separation in the event of tension developing between the soil and the wall. The slip elements were assigned Mohr-Coulomb properties with a friction angle of 20.7^{o}, which was measured in direct shear test. The cohesion was assumed to be zero. The layer of slip elements goes all the way around the retaining wall completely separating the soil from the retaining wall. The aspect ratio (vertical length/horizontal thickness) of the slip element was taken as 100. For this value of aspect ratio it has been shown by Pande and Sharma [15] that the analysis will be free of any numerical problems.

A modified version of the CRISP program [16], which included the slip element in the library of elements, was used in the analyses described in this paper.

Initial Stresses

In analyses of centrifuge model tests it is customary to use the stress state corresponding to the equilibrium conditions after reconsolidation in the centrifuge as the starting point. The stress history of one-dimensional consolidation is used to define the horizontal stress distribution with the aid of empirical relationships between OCR and K_{o}. In the current study, however, the stress conditions at this stage are complex. The zinc chloride contained in the rubber bag imposes a lateral

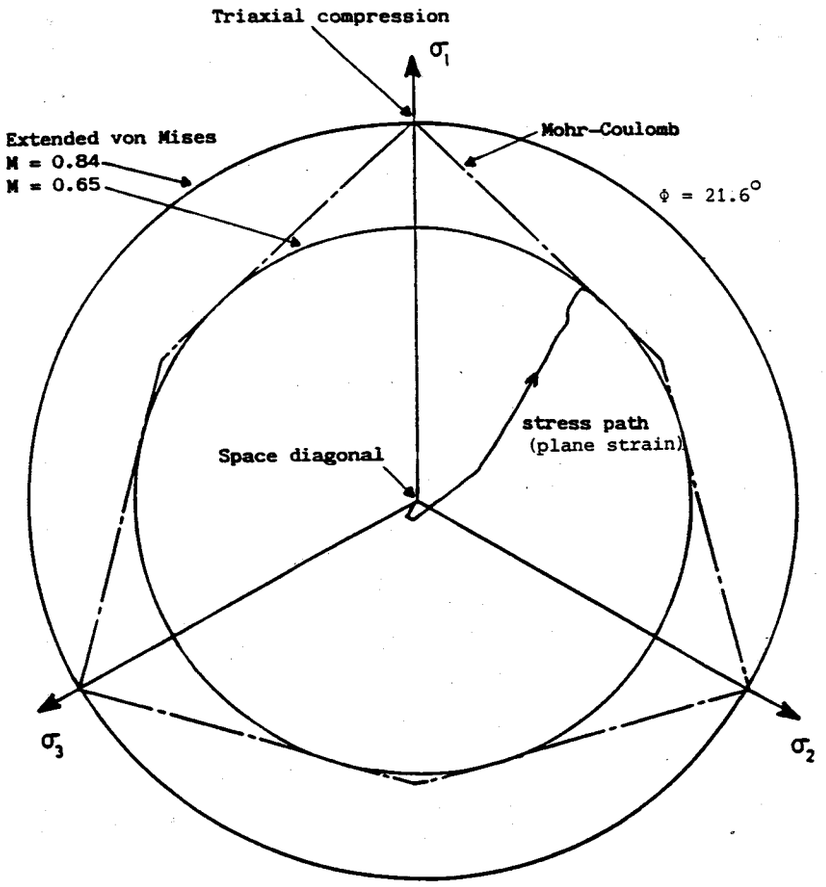

Figure 3 Typical stress path plotted in the deviatoric plane

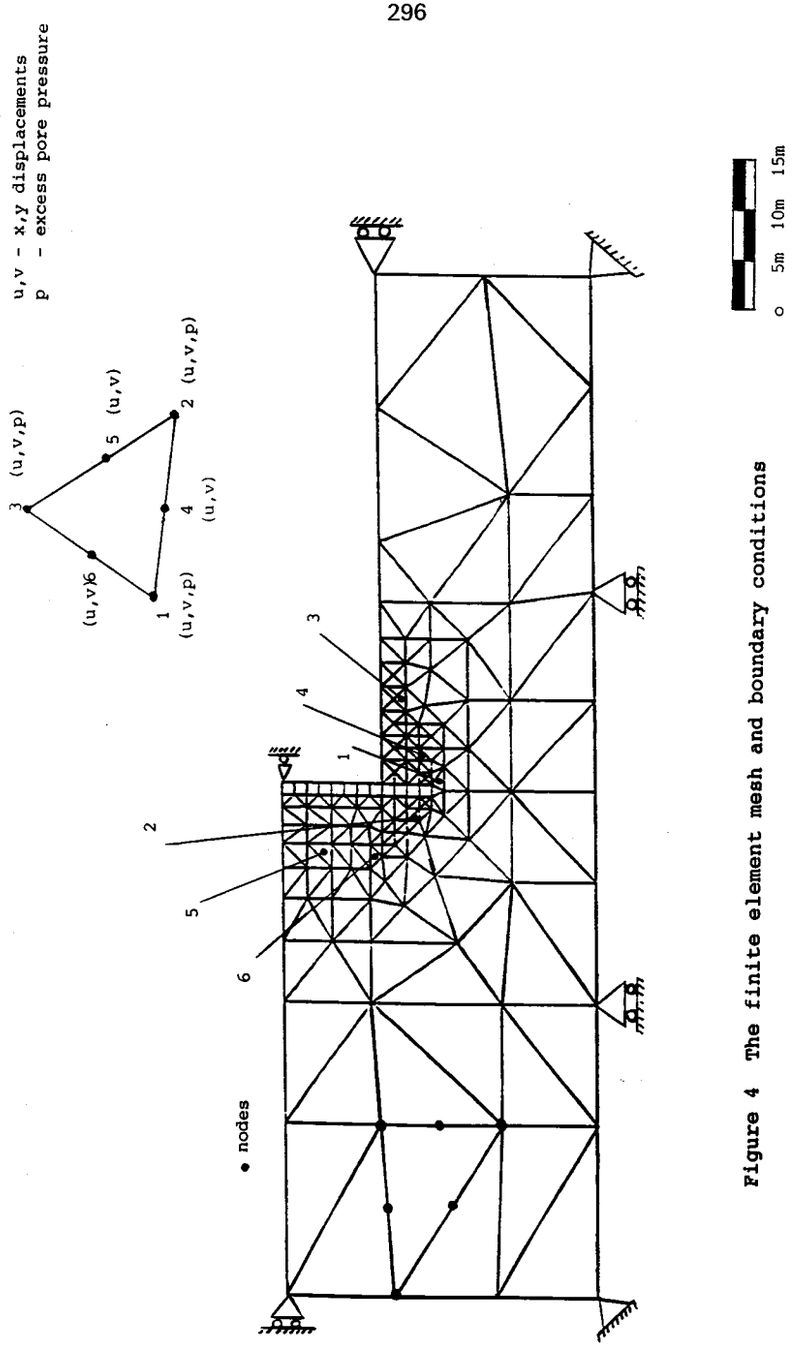

Figure 4 The finite element mesh and boundary conditions

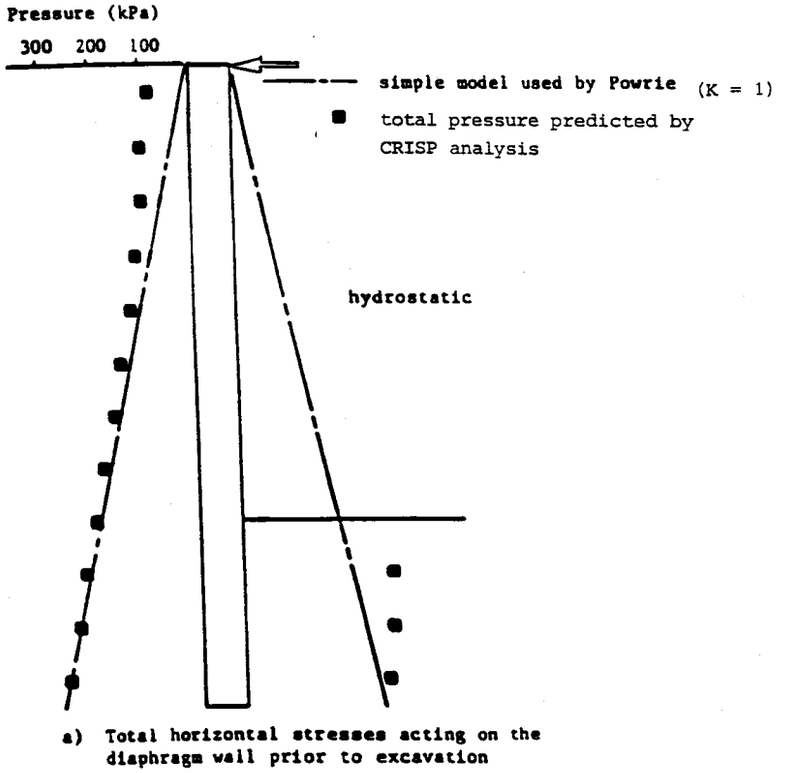

Figure 5 Initial stresses in the centrifuge model

earth pressure coefficient (K_0) of unity on the excavated side, but the presence of the diaphragm wall affects the distribution of the lateral stresses on the retained side. In order to make a prediction it was decided to use the state of the model at removal from the consolidation press as the starting point.

The sample was assumed to be in an isotropic state under a stress of 135 kPa in the consolidometer just prior to the removal of the vertical stress of 80 kPa. The removal of the vertical pressure of 80 kPa was simulated by removing this isotropic stress. The option within the CRISP program to apply gradually increasing gravity loading was used in the analysis. This simulates the gradual increase in centrifugal acceleration as the centrifuge is run up to full speed. In the analysis the boundary stress simulating the effect of the zinc chloride solution was increased in step to maintain overall equilibrium. Fig. 5 compares computed horizontal stress distribution with the assumption of $K_0 = 1$ used by Powrie [12]. The comparison is quite good, except close to the ground surface where the influence of swelling may be seen.

RESULTS OF THE FINITE ELEMENT ANALYSIS

Shear and Volumetric Strains

Contours of shear strain and volumetric strain after 7.38 years of prototype time, figures 6 and 7, show that significant swelling and shearing are restricted to a fairly well defined zone near the toe of the wall, and occur mainly on the passive side. Shear and volumetric strains in the remainder of the active region are small. Some shearing is also apparent at the soil-wall interface over the upper 40% or so of the retained height. The shear strains at the surface of the active zone are due to a predicted restraint of swelling as a result of friction at the soil/wall interface.

Excess Pore Pressures

On excavation negative excess pore pressures are computed in the active zone, figure 8, as the soil is forced to mobilise additional strength and yields with suppressed dilation. Pore water pressures in the passive region are subject to three effects, reduction due to loss of vertical total stress, increase due to the change of horizontal total stress demanded as the wall achieves equilibrium, and decrease due to the yielding of the "dry" clay : the net effect is marginal. The soil during this phase of the test behaves essentially in an undrained manner. After 7.38 years of prototype time, figure 9, the equilibrium flow net has largely established itself, with water flowing upwards into the excavation from the retained soil. In the areas of soil furthest from the drainage boundaries, most notably near the toe of the diaphragm wall, significant negative excess pore water pressures still exist.

Stress Paths

The stress paths followed by soil elements at various points in the model will now be discussed. Figure 4 shows the location of these points in the finite element mesh. Point 1, figure 10(a), is

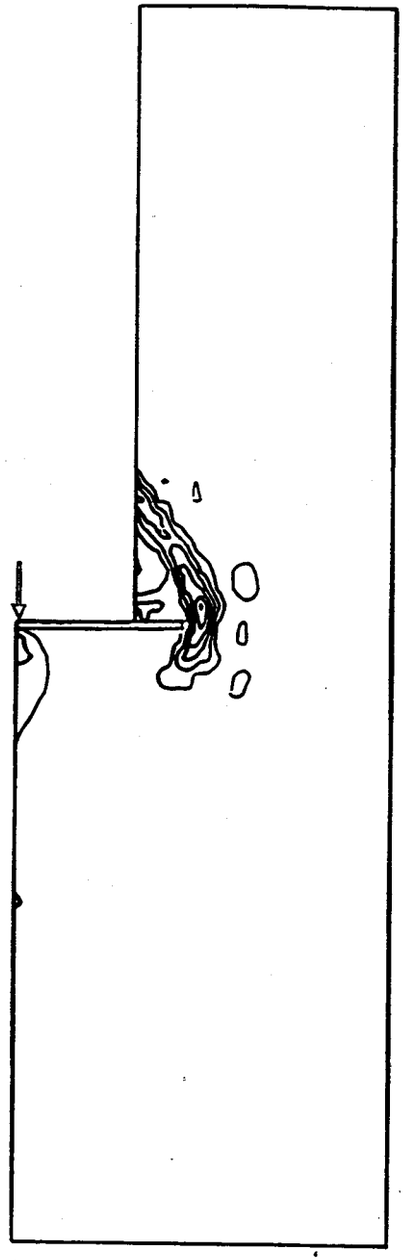

Figure 6 Computed shear strain contours 7.38 years (prototype time) after excavation

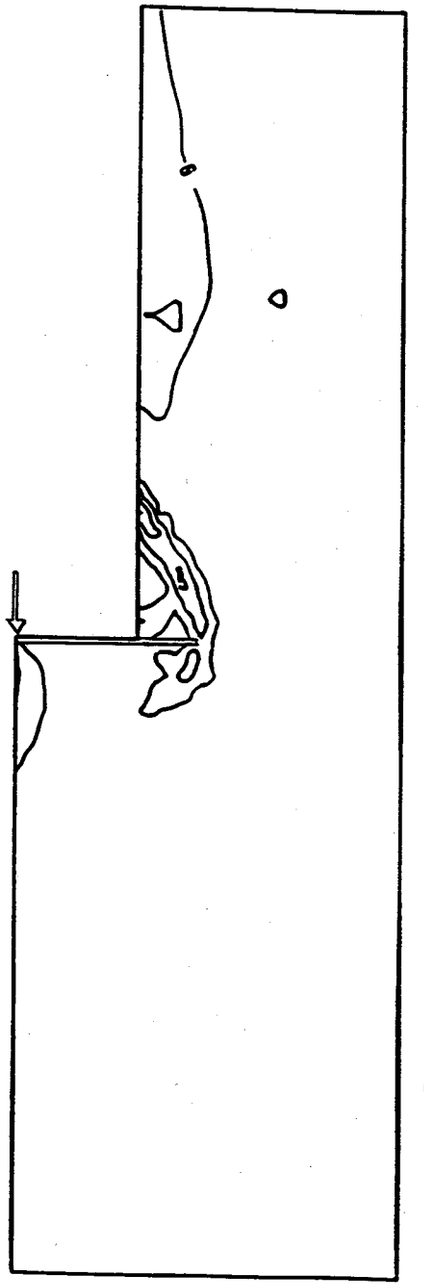

Figure 7 Computed volumetric strain contours 7.38 years (prototype time) after excavation

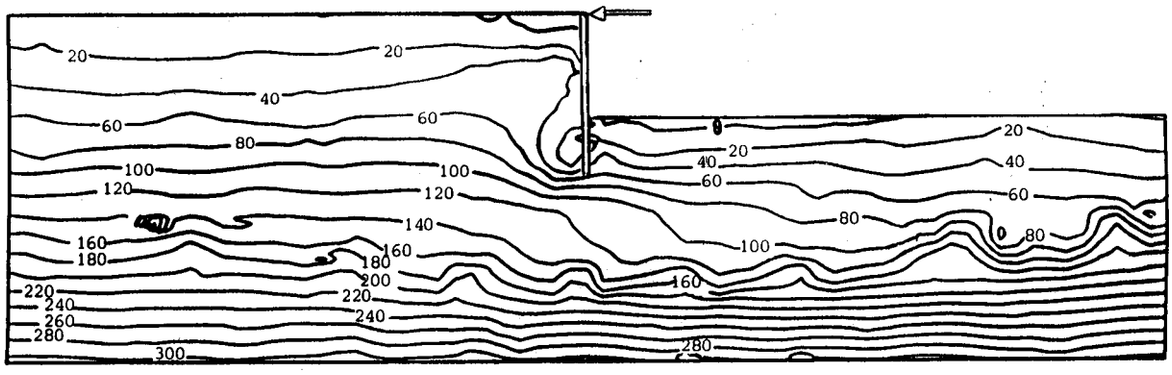

Figure 8 Computed total pore pressure contours at the end of excavation

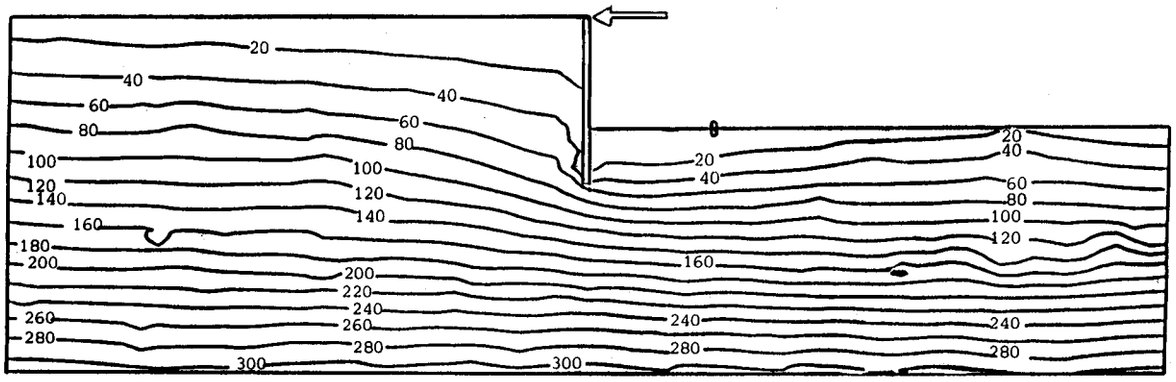

Figure 9 Computed total pore pressure contours 7.38 years (prototype time) after excavation

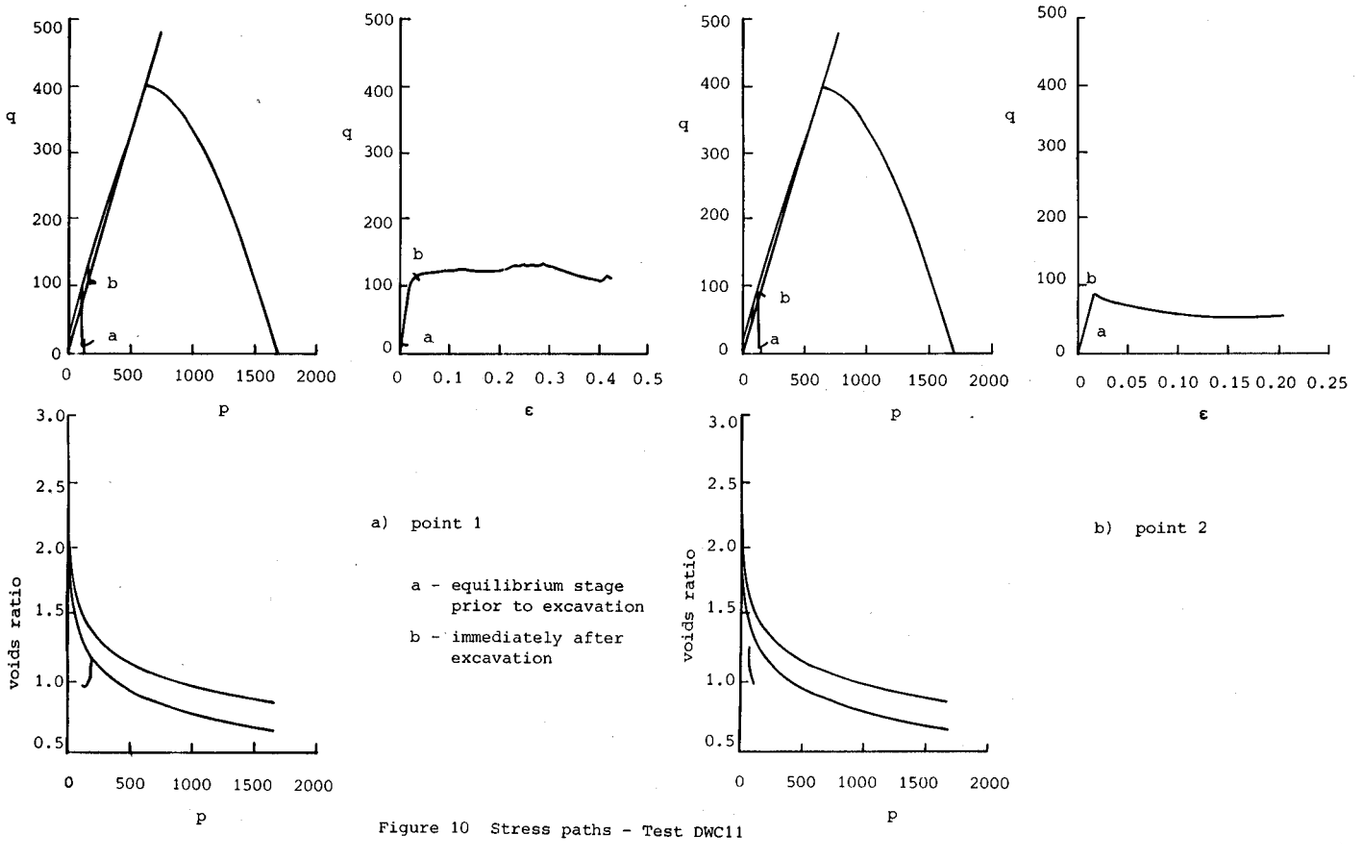

a) point 1

a - equilibrium stage prior to excavation

b - immediately after excavation

b) point 2

Figure 10 Stress paths - Test DWC11

located in front of the wall just below the toe, in a zone which ruptured during the centrifuge model test. The pore pressure rises as the speed of the centrifuge increased, and then gradually dissipates. The soil remains elastic during this phase. The dumping of the zinc chloride sees the stress state rise to the Hvorslev surface as the soil is sheared and the wall is forced to move to develop additional passive pressures. The stress path is characteristic of undrained loading, rising at constant mean effective stress to the yield surface. During the period of pore pressure dissipation which follows, the soil swells and softens, reducing the size of the yield locus. The stress state eventually approaches the critical state. At this stage, the shear stiffness has dropped to almost zero. As the negative excess pore pressures continue to dissipate, the stress state leaves the critical state and continues to soften on the Hvorslev surface.

The stress states of points 3 and 4, figures 11(a) and 11(b), in the developing shear band in the passive region, have progressed much of the way to the yield surface during the initial consolidation phase in the centrifuge. The dumping of the zinc chloride simulating excavation, then moves these points rapidly onto the Hvorslev surface. The subsequent period of excess pore pressure dissipation sees these stress states approach the critical state as the excess pore pressures dissipate and the soil swells. During the latter part of the dumping of the zinc chloride, the soil is forced to yield at constant volume, the volumetric expansion associated with yielding on the Hvorslev surface being suppressed by an increase in negative excess pore pressure. The stress points must therefore traverse a constant volume section of the Hvorslev surface and as the effective mean normal stress (p') increases due to the generation of negative pore water pressures the deviator stress continues to rise. This behaviour is associated with a reduction in the shear stiffness as plastic shear strains are also occurring. It is not necessarily characteristic of real soil which can rupture. Once the stress state is permitted to move off this constant volume section, during the period of excess pore pressure dissipation, the soil swells and the yield surface contracts. This results in a negative shear stiffness as the soil reduces in strength and is forced to shed load.

Points 2, 5 and 6, figures 10(b), 12(a) and 12(b), are all located in the active zone. All these points show only a small increase in deviator stress during the initial increase in the speed of the centrifuge and the subsequent consolidation phase. Point 2 alone then suffers a sufficient increase in deviator stress to take it onto the Hvorslev surface during the dumping of the zinc chloride. During the period of pore water pressure equilibration which follows excavation, all these points reach the Hvorslev surface where volumetric swelling and reduction in the size of the yield surface occurs. All points are heading towards the critical state line, the closer the points are to the surface of the centrifuge model the more remote their stress states from the critical state line.

Yield Zones

The computed distribution of yielding in the model after completion of excavation is shown in figure 13(a). An extensive area of soil has begun to yield, on the Hvorslev surface, in the passive zone as it is forced to carry the load previously supported by the zinc chloride. This is due to a

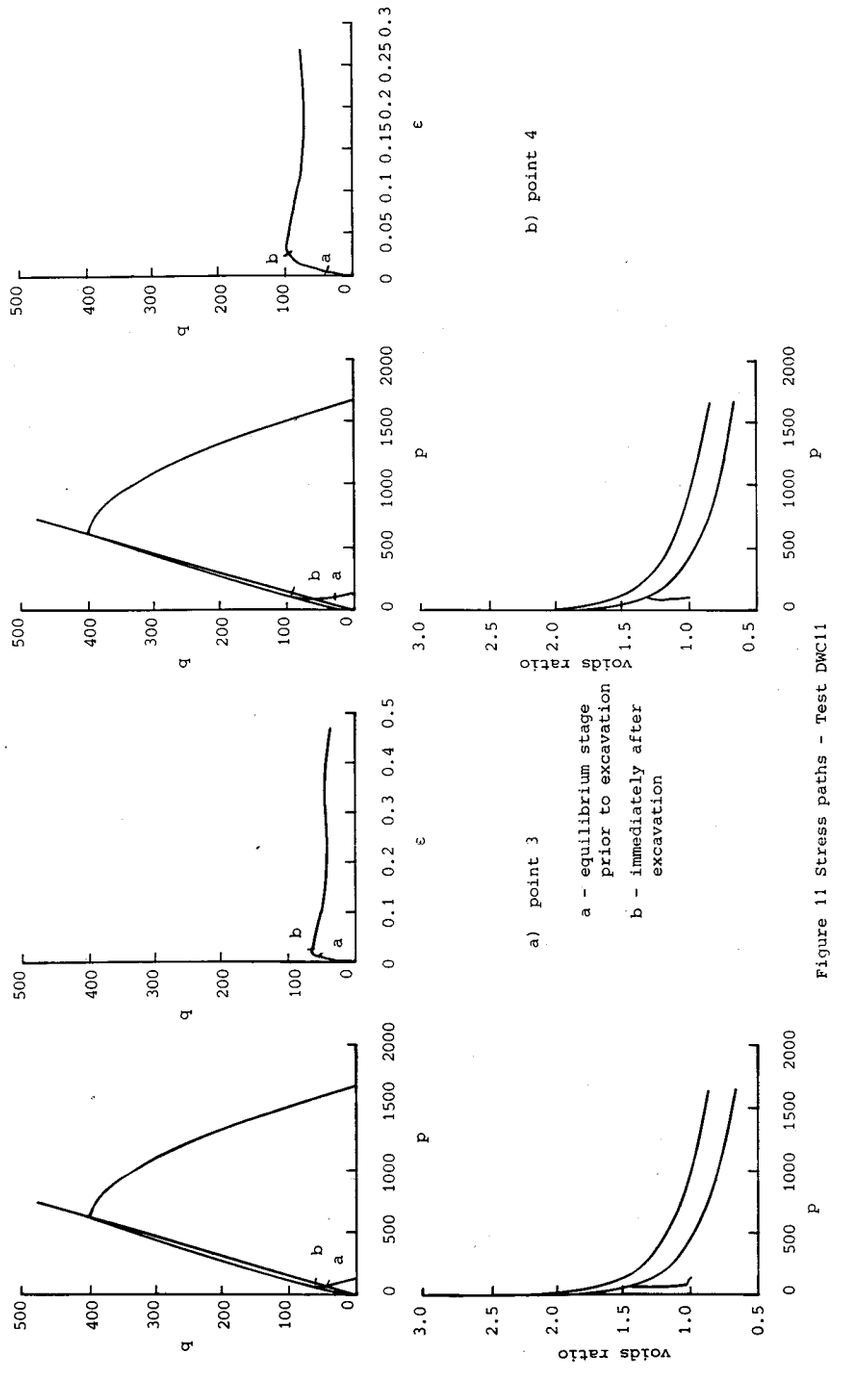

Figure 11 Stress paths - Test DWC11

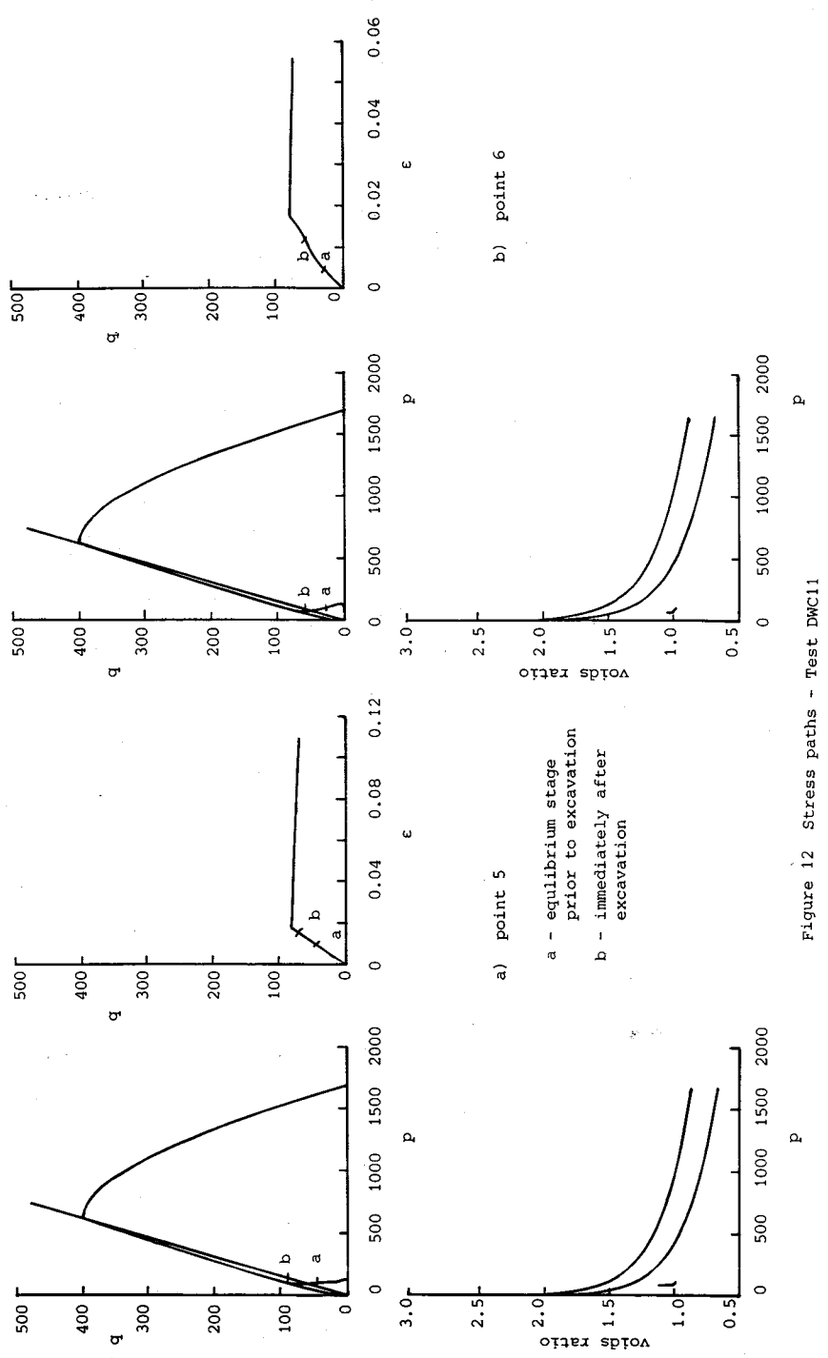

Figure 12 Stress paths - Test DWC11

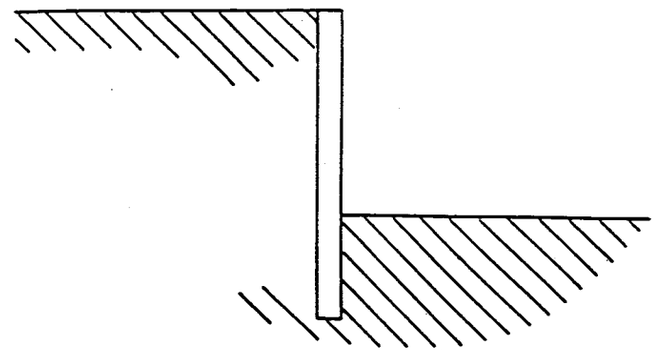

(a) end of excavation

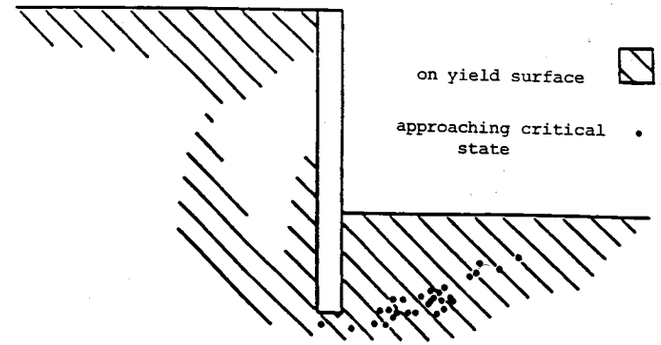

(b) 7.38 years (prototype time) after end of excavation

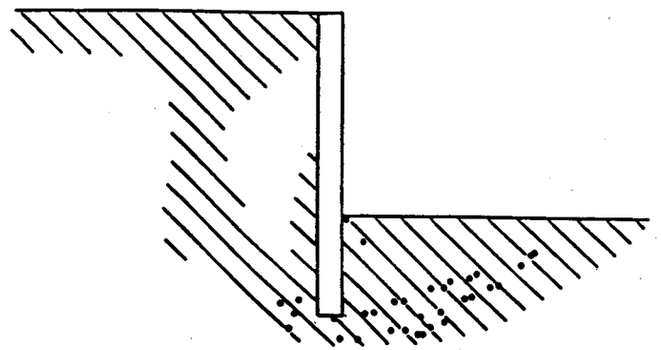

(c) 10.38 years (prototype time) after end of excavation

Figure 13 Extent of zones at particular stress conditions during the analysis

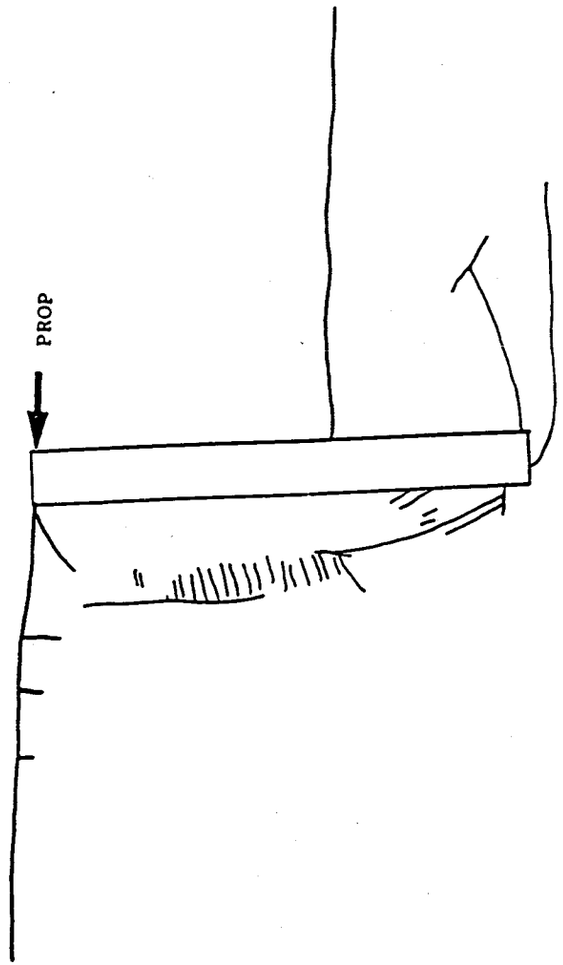

Figure 14 Rupture patterns observed at the end model test DWC11 (from Powrie, 1986)

combination of unloading and the support provided for the wall. The zone of yielding extends under the toe of the wall and into the active zone but is confined to a very limited area. The soil near the ground surface continues to swell as the remaining negative excess pore pressures continue to dissipate.

After 7.38 years prototype time have elapsed, figure 13(b), the zone of yielding on the passive side of the wall has extended. A limited and quite well defined zone of soil is approaching critical states in a band extending from just below the toe of the wall towards the surface of the excavation at a shallow angle : this delineates the zone of impending passive failure. On the active side, the zone of yielding extends in a continuous band to the soil surface. All of the soil at yield is swelling and softening. A localised zone of yielding also extends up the wall : this is associated with the continuing reduction in horizontal effective stress as the wall moves forward.

By 10.38 years prototype time, figure 13(c), the extent of the zones of yielding has changed little, but the band of soil approaching critical states has now altered, with two lines of failure appearing to propagate from the toe of the diaphragm wall into the passive zone, one extending horizontally from just below the toe level of the wall and the other progressing towards the surface at a shallow angle. These zones of soil approaching failure on the excavated side of the wall display a very good correspondence with the rupture zones in this region reported by Powrie [12], figure 14.

A number of points on the retained side have also begun to approach critical states, but the zone of impending failure is not yet discernible. The analysis became unstable shortly after this and it was therefore not possible to follow the progress of the rupture through the active region. A significant area of soil in the active zone is still elastic. In real soil, when a stress path reaches the Hvorslev surface the soil ruptures in thin layers. In kaolin these are typically 20-100 microns thick [17], permitting much faster dissipation of negative excess pore pressures and softening as the clay shears. In the analysis, the zone of yielding is much thicker and the pore pressures must dissipate over much larger areas and consequently over a much longer time due to the drainage path lengths involved. This could explain the more ductile behaviour of the active zone in the finite element model relative to the centrifuge model.

COMPARISON WITH CENTRIFUGE MODEL TEST DATA

The locations of the transducers in the centrifuge model are shown in Fig. 15.

Displacements

Fig. 16 compares the measured and computed soil displacements during dumping of the zinc chloride solution. The computed displacements are generally larger and more extensive than the measured, and also correspond more obviously to a rotation of the wall about the position of the prop. The same is true of the displacements after 7.38 years would have elapsed at prototype scale, Fig. 17. It is also apparent from Fig. 17 that the analysis overpredicts the magnitude of the heave of the excavated soil surface and fails to predict the quite large settlements which occurred near the

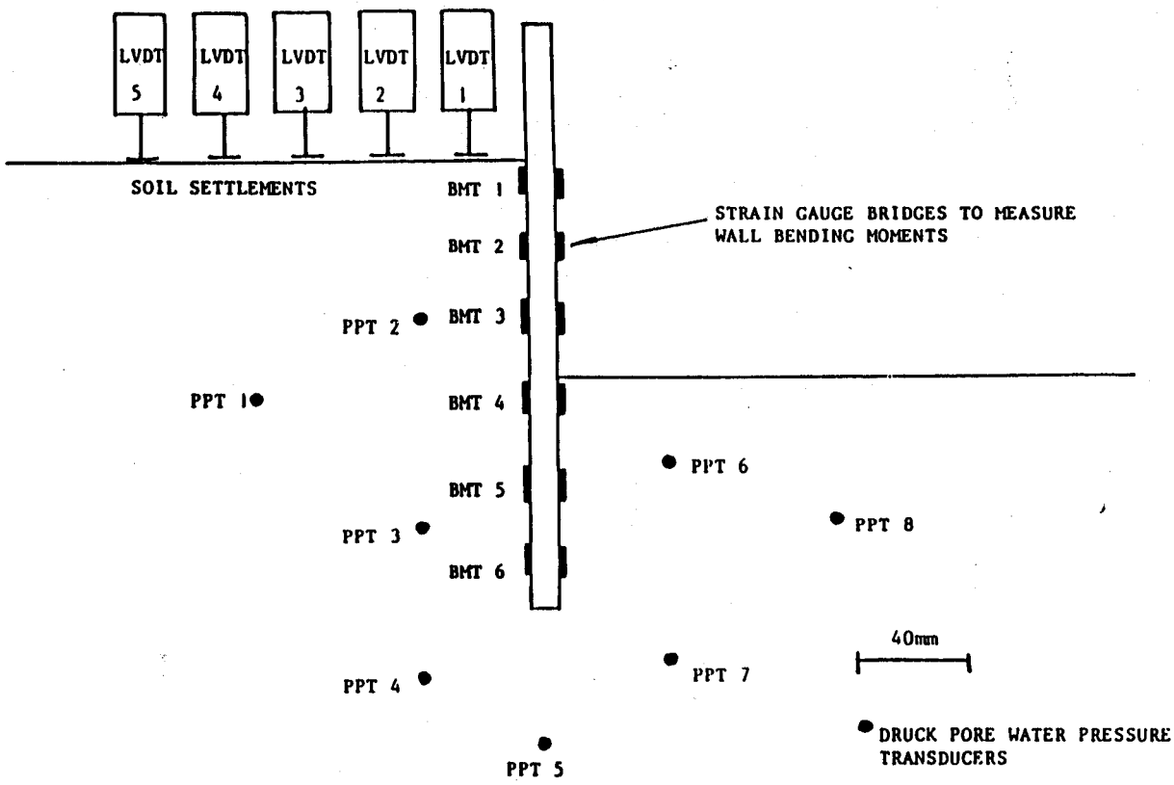

Figure 15 **Layout of instrumentation in model test DWC11 (from Bolton and Powrie, 1987)**

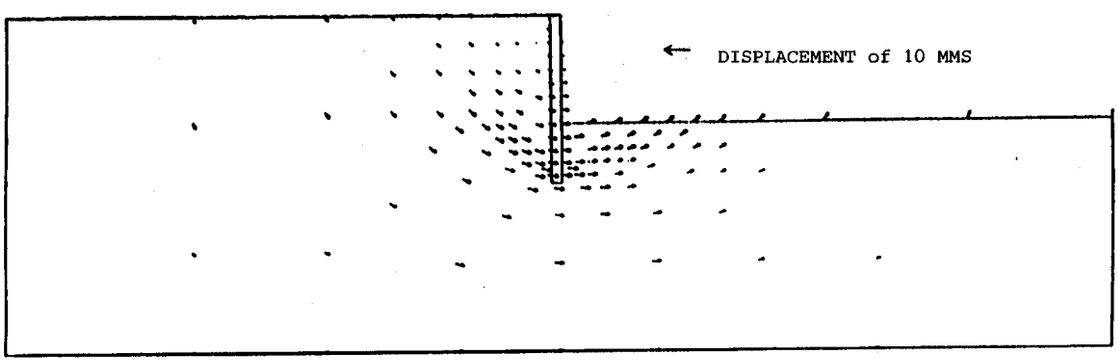

(a) Computed

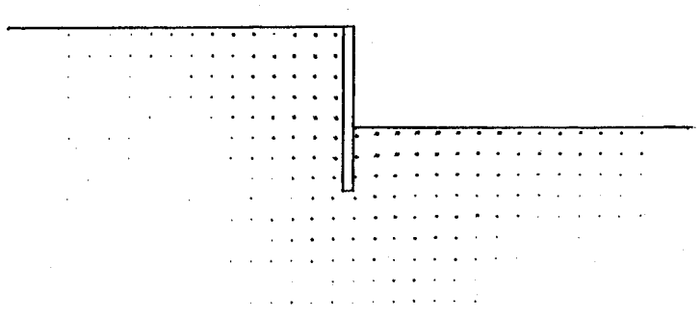

(b) Measured

Figure 16 Computed and measured displacements at the end of excavation

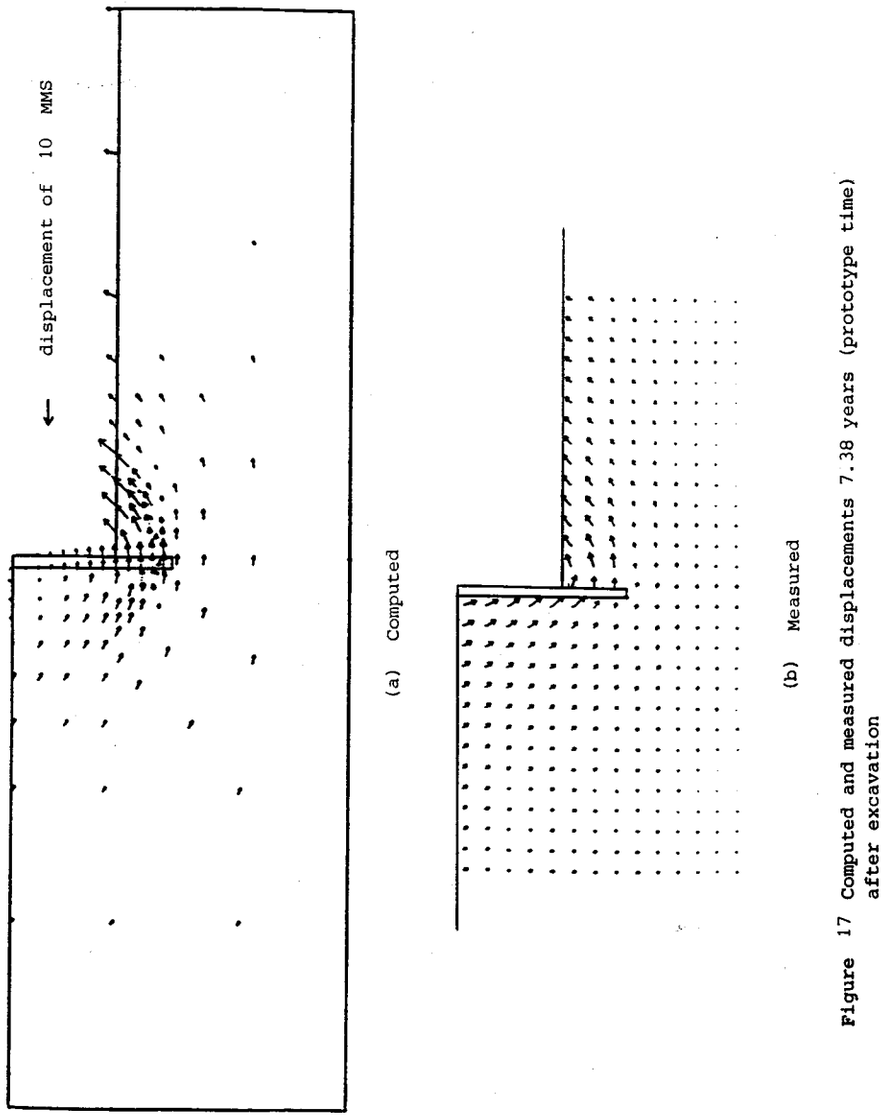

Figure 17 Computed and measured displacements 7.38 years (prototype time) after excavation

wall on the retained side in the centrifuge model test, the computed displacements in this region being virtually horizontal.

Comparison of the measured and computed incremental soil movements occurring after excavation (Fig. 18) suggests that the principal sources of descrepancy are

(1) the overprediction of the elastic components of the computed deformations, and

(2) the absence in the analysis of anything corresponding to the active side rupture, sliding along which clearly influenced the displacement pattern observed in the centrifuge model.

In the analysis, the shear modulus G was calculated from a constant Poisson's ratio of $\nu' = 0.33$ and an effective bulk modulus $K = (1 + e)p'/\kappa$ where p' is the current mean normal effective stress,

$$G = \frac{3(1 - 2\nu')(1 + e)p'}{2(1 + \nu')\kappa} \qquad (1)$$

It is generally accepted [18,19,12] that the secant shear modulus is initially high, but reduces gradually with increasing shear strain (Fig. 19).

It may seem that the use of equation 1. (assuming p' = constant : Fig. 19) underpredicts the shear modulus at low strains. It is therefore not surprising that the elastic strains predicted by the current analysis are too large : For example, Fig. 13 shows that at the end of the excavation phase the behaviour of the soil on the retained side is still predominantly elastic, and the computed displacements of the wall at formation level is twice as high as the measured value.

Pore Water Pressures

The pattern and magnitude of the response of 8 pore water pressure transducers, Figs. 20 and 21 shows generally good correlation with the numerical prediction both in the passive and active zones.

Bending Moments and Prop Force

Fig. 22 compares the measured and computed bending moments. The computed bending moments are much higher. This may be because the retained soil mobilises more strength than computed by the analysis. The prop was modelled as rigid in the analysis, whereas the prop used in the centrifuge test would have compressed slightly, permitting the mobilisation of a higher soil strength and a corresponding reduction in lateral earth pressure coefficients.

The prop force due to excavation measured in the test corresponded to 453 kN per metre length of the wall at prototype scale. This may be compared with the computed value of 588 kN/m which is similarly an overestimate.

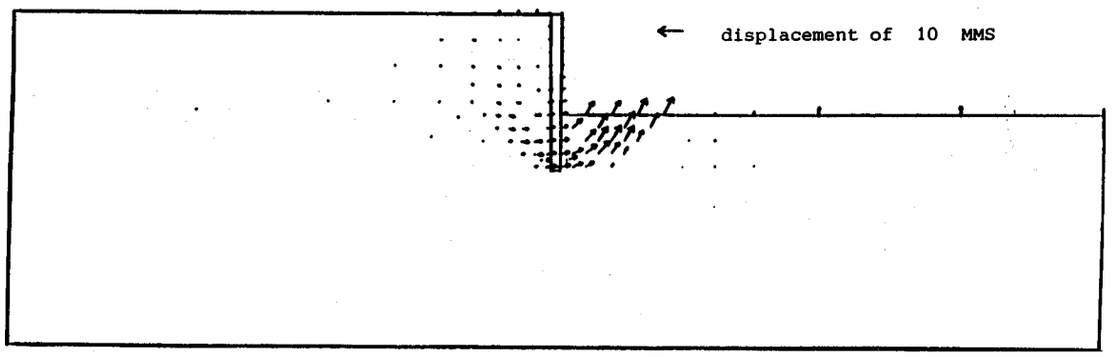

(a) Computed

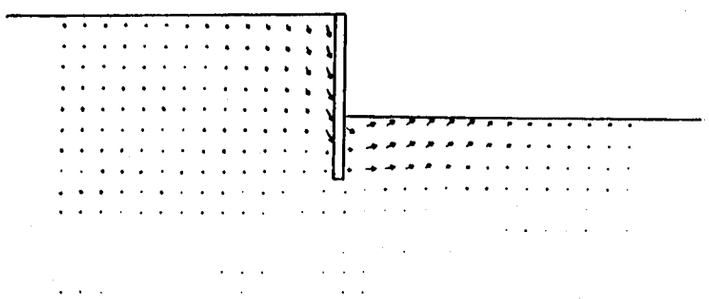

(b) Measured

Figure 18 Computed and measured post-excavation soil movements

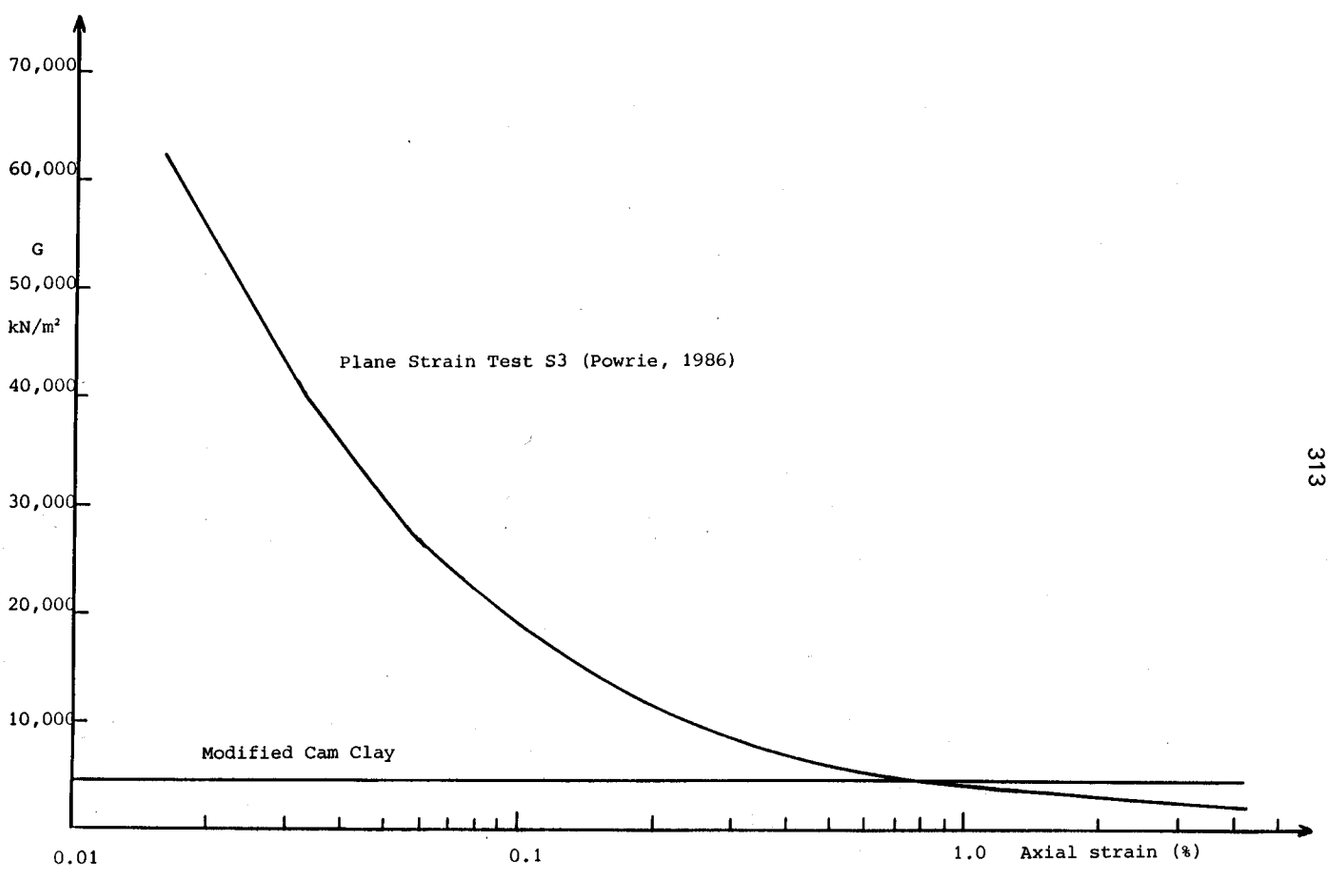

Figure 19 Measured and computed shear modulus

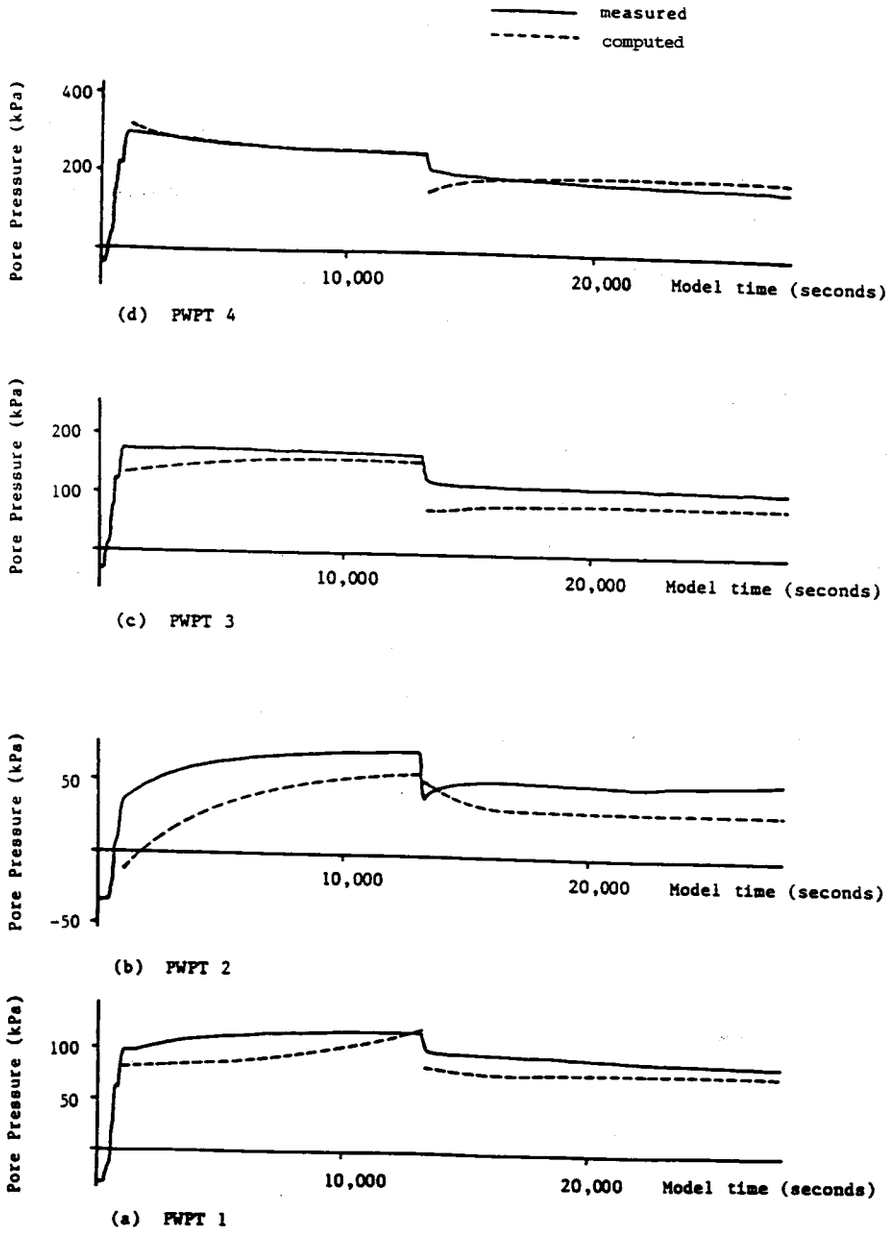

Figure 20 Computed and measured pore pressure response versus time

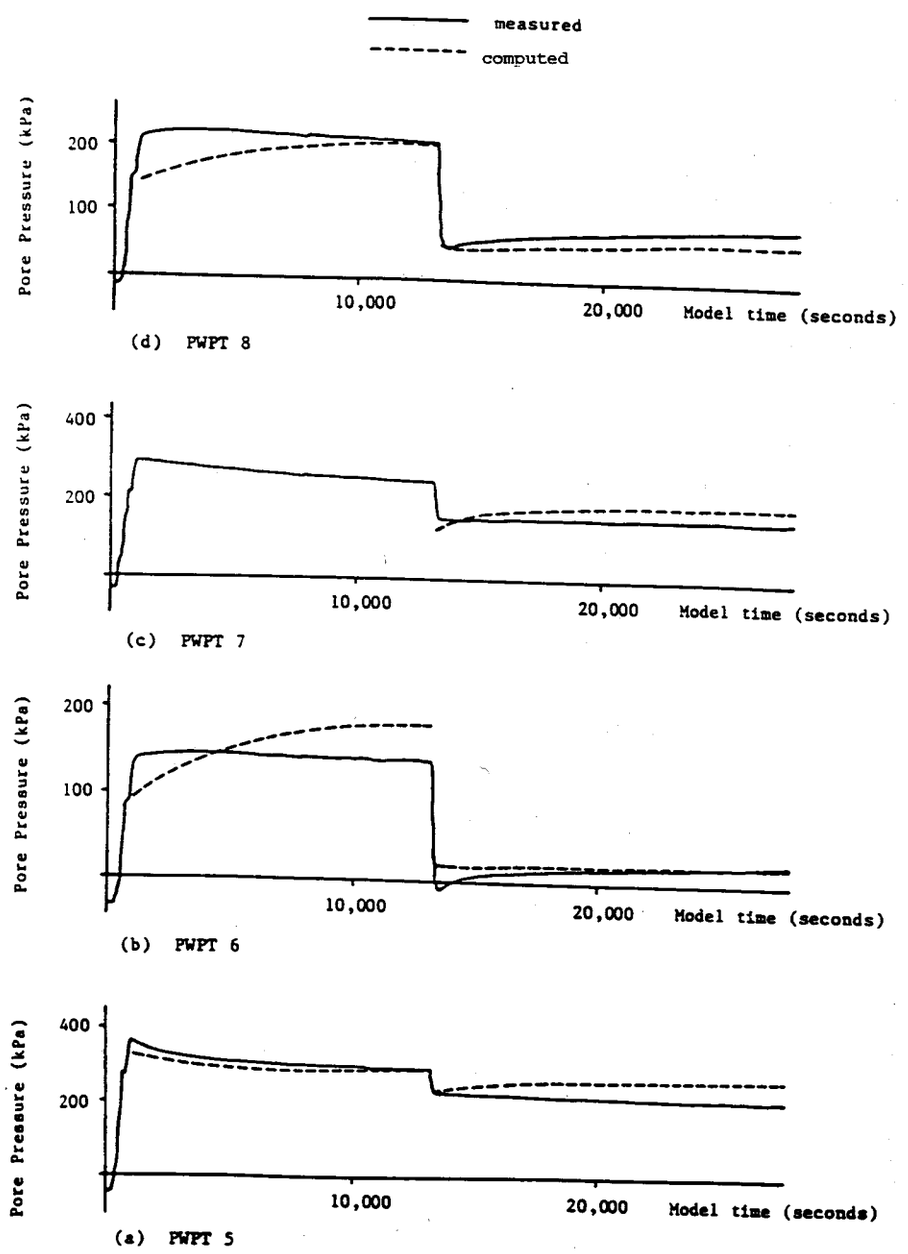

Figure 21 Computed and measured pore pressure response versus time

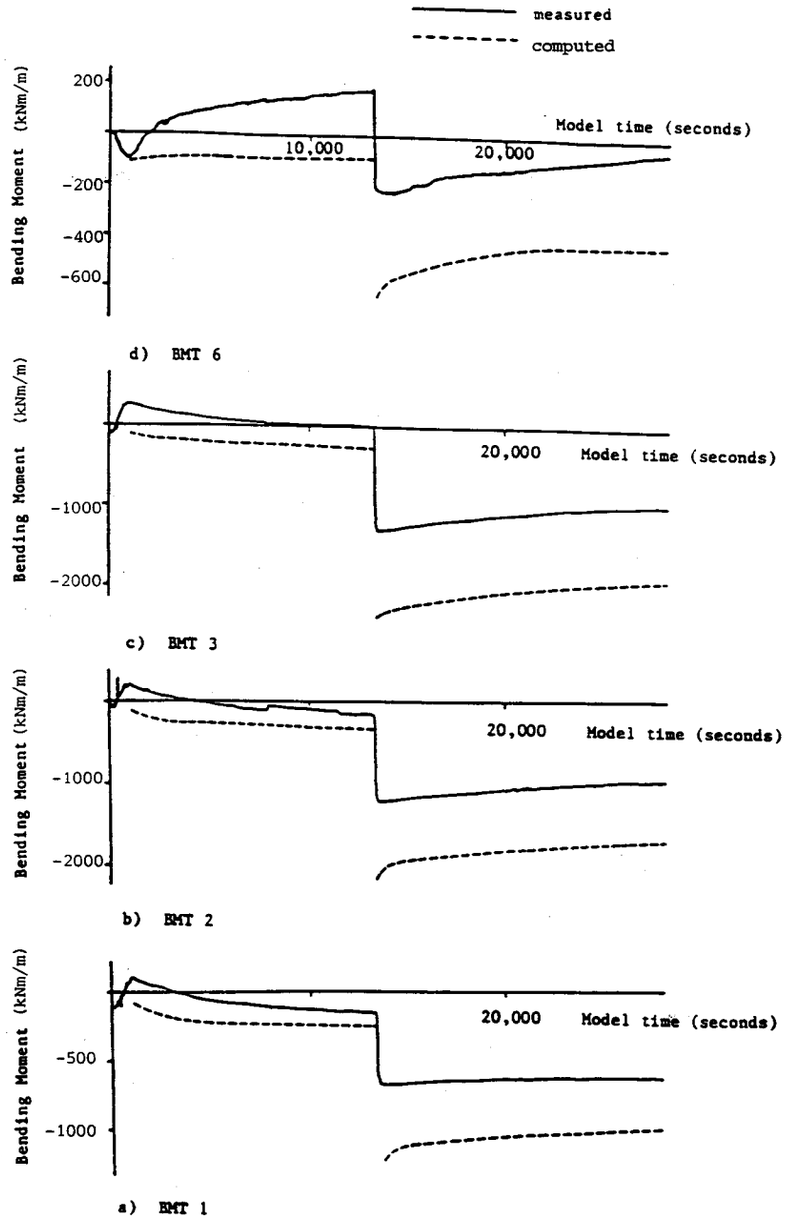

Figure 22 Computed and measured bending moments in the diaphragm wall versus time

CONCLUSIONS

The computed pattern of localised yielding and the resulting displacements agreed well with the observed behaviour in the passive zone. In the analysis, two lines of failure appeared to propagate from the toe of the wall into the passive zone, one horizontally and the other progressing towards the surface at a shallow angle. These zones of soil approaching failure corresponded well with the rupture zones observed in the centrifuge test. However the inability to model the rupturing of the soil in thin layers on the Hvorslev surface in a continuum type analysis may account for the differences observed in the active zone.

However, the time scale to rupture computed by the analysis was rather longer than that observed in the centrifuge model test. This is largely due to the assumption of a continuum implicit in the finite element analysis, which cannot model the formation of ruptures as would be expected in a real soil on the Hvorslev surface. The analysis became unstable before the failure zone in the active region had fully developed.

Pore pressures were reasonably well simulated but bending moments in the diaphragm wall were overpredicted by a factor of 2. The displacements were correspondingly overpredicted by CRISP at the end of the excavation process, when most of the active zone is still elastic and the shear modulus has a much more significant influence on the displacements than any other parameter. A stiffer representation of small-strain behaviour in the contained active zone would have led to a greater mobilisation of soil strength, and correspondingly reduced structural load effects, more in accordance with the observations of the physical model.

The assumption made by Powrie [12] of K_o equal to 1.0 for the calculation of initial stresses on the wall was well supported by the analysis except near the surface where additional pressures due to the swelling of the surface soil was computed.

ACKNOWLEDGEMENTS

The first two authors were employed by the University of Cambridge. The work reported herein was carried out under research contracts placed by the Transport and Road Research Laboratory. The views expressed are not necessarily those of the Department of Transport.

The third author received support from the Science and Engineering Research Council and the fourth author from the Robert Gleddon Overseas Fellowship and the Main Roads Dept of Western Australia Highway Authority.

REFERENCES

1. Schofield A.N. and C.P. Wroth Critical State Soil Mechanics, McGraw Hill, London (1968).

2. Wroth C.P., The predicted performance of soft clay under a trial embankment loading based on the Cam-Clay model, in Finite Elements in Geomechanics, Edited by G. Gudehus,

John Wiley (1977) Chapter 6.

3. Almeida M.S.S., Stage constructed embankments on soft clays, Ph.D. thesis, Cambridge University (1984).

4. Almeida M.S.S., A.M.Britto and R.H.G.Parry
Numerical modelling of a centrifuged embankment on soft clay, Canadian Geotechnical Journal, **23** (1986) 103-114.

5. Bolton M.D. and Powrie W.,
The collapse of diaphragm walls retaining clay,
Geotechnique Vol. 37 (1987) 335-353.

6. Schofield A.N., Cambridge geotechnical centrifuge operations, Twentieth Rankine Lecture,
Geotechnique, Vol 20 No 2 (1980) 129-170.

7. Al-Tabbaa A., Permeability and stress-strain response of Speswhite kaolin, Ph D thesis, Cambridge University (1987).

8. Phillips R., Ground deformations in the vicinity of a trench heading, Ph D thesis, Cambridge University (1987).

9. Nadarajah V., Stress-strain properties of lightly overconsolidated clays, Ph D thesis, Cambridge University (1973).

10. Al-Tabbaa A. and Wood D.M.,
Some measurements of the permeability of kaolin,
Geotechnique, Vol. 37 (1987) 499-503.

11. Mair R.J., Centrifugal modelling of tunnel construction in soft clay, Ph.D. thesis, Cambridge University (1979).

12. Powrie W., The behaviour of diaphragm walls in clay, Ph D thesis, Cambridge University (1986).

13. Stewart D.I., Ground water effects on in situ walls in stiff clay, (forthcoming) Ph D thesis, Cambridge University (1989).

14. White T.P., Finite element calculations involving the yielding of dilatant soils, M.Phil thesis, Cambridge University (1987).

15. Pande G.N. and K.G.Sharma
On joint/interface elements and associated problems of numerical ill-conditioning.
Int. Jl. of Num. Anal. Meth. Geomech., **3** (1979) 293-300.

16. Britto A.M. and M.J.Gunn
Critical State Soil Mechanics via Finite Elements,
Ellis Horwood, Chichester (1987).

17. Wong K.Y., Micro-fabric changes during the deformation of clays, Ph D thesis, Cambridge University (1976).

18. Jardine R.J., M.J.Symes and J.B.Burland
Measurement of soil stiffness in the triaxial apparatus.
Geotechnique, Vol 34 No 3 (1984) 323-340.

19. Jardine R.J., D.M. Potts , A.B.Fourie and J.B.Burland
Study of the influence of non-linear stress-strain characteristics in soil-structure interaction,
Geotechnique, Vol 36 No 3 (1986) 377-396.

Received 15 May 1989; revised version received 21 August 1989; accepted 23 September 1989